Modeling and development of an auxetic foam-based multimodal capacitive strain gauge

OPEN ACCESS
IOP Publishing
Smart Materials and Structures
Smart Mater. Struct. **32** (2023) 025013 (12pp)
https://doi.org/10.1088/1361-665X/acafb7

Modeling and development of an auxetic foam-based multimodal capacitive strain gauge

F Rizzi[1,4,*], S Puce[1,2,4], F La Malfa[1,2], M Totaro[3], M De Vittorio[1,2,4] and L Beccai[3,4]

[1] Center for Biomolecular Nanotechnologies, Istituto Italiano di Tecnologia (IIT-CBN), Lecce, Italy
[2] Dipartimento di Ingegneria dell'Innovazione, Università del Salento, Lecce, Italy
[3] Soft BioRobotics Perception Lab, Istituto Italiano di Tecnologia, Genova, Italy

E-mail: francesco.rizzi@iit.it

Received 4 August 2022, revised 30 November 2022
Accepted for publication 2 January 2023
Published 20 January 2023

Abstract

Auxetics are mechanical metamaterials with the unique properties of expanding their transversal section upon longitudinal positive strain, decoupling the deformations in normal and transversal directions. Such property can be exploited to develop soft sensors that can provide feedback to different mechanical stimuli, e.g. pressure and shear force. In this work, we propose for the first time a mathematical model to analytically simulate and design the auxetic behavior in a capacitive strain gauge, and show that, for a polyurethane (PU) auxetic foam, Poisson Ratio's values can satisfy the negative gauge factor (GF) condition. We develop an innovative thermo-compressive process to obtain anisotropic auxetic PU sponges both in normal and normal/radial directions, and their mechanical properties are in agreement with the theoretical calculations validating our model. Then, we develop a capacitive strain gauge by integrating a normal auxetic PU foam with polydimethylsiloxane /carbon nanotubes electrodes. Results show that the capacitive change caused by an external force, is proportional to the induced deformation, but importantly it is also dependent on the direction of the applied force. A negative GF of $GF = -2.8$ is obtained for a longitudinal strain range up to 10%. This auxetic foam structure guarantees flexibility and paves the way for an improved design freedom for multimodal mechanical soft sensors providing new opportunities towards smart wearables and perceptive soft robots.

Supplementary material for this article is available online

Keywords: auxetic, foam, strain gauge, multimodal

(Some figures may appear in colour only in the online journal)

[4] These authors contributed equally to this work.
[*] Author to whom any correspondence should be addressed.

1. Introduction

Auxetic materials are mechanical metamaterials with unique properties resulting from their structure. Their elastic properties, such as shear modulus, compression and absorption resistance, can be controlled by designing a complex structure constituted by elementary-cells whose mechanical deformation results in a negative Poisson's ratio [1–3]. When auxetic materials are stretched in the longitudinal direction, they become thicker in one or several of the perpendicular widthwise directions, while, when they are subjected to uniaxial compression, they display a thinning in one or several of the transverse directions. This behavior is due to the numerous hinge-like cells that constitute the auxetic material and that are joined together [4]. Under tension, thanks to a re-entrant geometry, the elementary cell expands in lateral direction.

Auxetic materials can be found in nature or artificially synthetized, and they scale from molecular size to macroscopic level, since the auxetic behavior is a scale-independent property [5, 6]. Such materials are known to absorb vibrations, and can enhance strength and resilience to shear forces; e.g. in the construction sector, they can be used to manufacture new fasteners and nails, which undergo lateral contraction during compression to assist the insertion [7, 8]. Furthermore, auxetic materials can be used for developing highly responsive piezoelectric sensors or actuators with distributed shunted piezoelectric patches [9]. When employed as electrodes sandwiching a polymer, they cause its lateral contraction in response to a compressive load. This way the sensitivity of the device increases by at least a factor of two, and possibly by ten or a hundred times, because the device performance depends on electromechanical coupling [10]. Other utilizations include smart mechanical filters, made with an auxetic material that can stretch tuning the passage pressure, and thus clean the pores by flushing the dirt out with water or other fluids [11]. Also, auxetic materials improve the acoustic-to-electric energy conversion [12], and the low bulk modulus makes them more sensitive to hydrostatic pressure.

At the microscale, very interesting applications can be addressed by building nano- or micro-electro-mechanical-systems based on buckling-induced Kirigami. In the latter, after uniaxial in-plane tension, an out-of-plane deformation is induced whose extension is controlled by load magnitude [13, 14]. This is obtained through auxetic materials that can expand in the direction perpendicular to an externally exerted tension and depending on load applied along an in-plane direction [15].

The auxetic mechanism can be very useful in soft mechanical sensing for pursuing perceptive soft robotic systems [16]. Indeed, adding mechanical controllable anisotropic behaviors in soft tactile sensors can be very useful to design devices that can respond to different mechanical stimuli from different directions, e.g. those originated either from the outer world or from the movement of the soft robot itself or in a wearable device. In this vision, it is important to design auxetic materials having well defined mechanical characteristics, such as stretchability and Poisson's ratio. A perforated auxetic mesh structure could simultaneously induce stretching in two orthogonal directions upon tensile loading and can be placed on highly deformable areas of the human body, such as the forearms and palms [17]. Strain gauge sensors based on two-dimensional (2D) auxetic materials were obtained through conductivity changes in a laser-etched auxetic silicone functionalized on which polyethyleniminereduced graphene oxide nanocomposite layers were constructed through a self-assembling process [18]. Two-dimensional printing techniques were also exploited for obtaining an auxetic re-entrant structure in a silicone rubber mixed with chopped carbon fibers [19], in polydimethylsiloxane (PDMS) mixed with carbon-based conductive thermoplastic elastomer fibers [20] or carbon-black-doped Ecoflex silicone rubber (CB/Ecoflex) [21]. In parallel, 2D strain gauges based on capacitance changes provoked by strain induced deformations in the sensor's geometry were addressed. The auxetic behavior was obtained by carefully cutting the starting elastomeric material with re-entrant structure, embedded between PEDOT:PSS organogel electrodes [22] or between liquid metal (eutectic gallium–indium) electrodes [23]. Alternatively, the auxetic soft dielectric was textured from embossed geometries forming lattices [24]. Due to their inherent 2D design, all these devices resulted auxetic only in longitudinal direction.

Sensitivity in transversal direction can be obtained exploiting three-dimensional (3D) structured materials or, more easily, through auxetic sponges. Conventional sponges, with a positive Poisson's ratio and open cells, are good candidates for the conversion into auxetic ones as reported by a large number of works in the literature [25, 26]. It is possible to obtain an isotropic auxetic sponge starting from a reticulated polyurethane (PU) foam with a uniform open cell distribution. A common PU sponge can be converted into an auxetic one in the three dimensions trough a thermal compression process that modifies the regular convex cells in the PU honeycomb structure creating a 3D re-entrant cells topology in which the ribs protrude inwardly. Re-entrant ribs easily explain how auxetic PU foams work: under tension the re-entrant cells tend to move out and when compression is applied, the ribs will bend further inward, resulting in a lateral contraction [1, 27, 28]. PU-based auxetic foams were applied to different types of stretchable strain gauges, such as a triboeletric-based strain gauge [29] and a piezoresistive strain gauge based on carbon nanotube (CNT)-functionalized open-cell auxetic PU foam [30].

However, for designing the sensors, modeling of auxetic strain gauges is of paramount importance. Finite element methods (FEM) [31] or a simple electromechanical models [32] were applied to describe reentrant geometric struts of artificial auxetic materials. A Poisson's function and a tangent Poisson's function formulation combined with FEM [33] were used to describe a 3D foam but, since the foam was considered homogeneous, only 2D models were implemented. To the authors' knowledge, up to date a model describing a 3D auxetic sponge-based strain gauge has not yet been developed. In this work, an innovative way to design and achieve an anisotropic thin auxetic PU sponge is presented and used as the

dielectric layer in a strain capacitive sensor, including modeling and its validation. In the first section, an effective model to set the conditions for the materials' auxetization (in order to obtain a negative gauge factor (GF)) is presented for the first time. It shows that materials with a negative Poisson ratio's value in different geometric direction, such as auxetics, can be exploited for a strain gauge sensor with negative GFs. In the second section, PU material and its thermo-mechanical auxetization methods are reported, and a new multi-strain compression technique for fabricating auxetics in normal and normal/radial direction is realized. The third section is focused on the dynamic electro-mechanical analysis (DMA) of the auxetized sponges in order to evaluate the transversal Poisson's ratio. The fabrication and characterization of a capacitive strain sensor is shown, paving the way for a multimodal sensor design. Finally, the model describing the auxetic sponge-based capacitive strain gauge is validated.

2. Modeling for negative GF in an auxetic capacitive strain gauge

Exploiting strain is the most common technique for retrieving mechanical cues in soft/hybrid systems. In strain sensors basically a change in either the electrical resistance or capacitance is measured, due to applied forces [34]. In a capacitive-based strain sensor if the dielectric layer consists of an auxetic material a non-conventional behavior is shown: if longitudinally stressed, this material reacts with an out of plane expansion and, consequently, the distance between the two plates of the capacitor increases, decreasing the capacitance value. This behavior is the opposite of the expected deformation, which decreases the capacitor thickness and increases the capacitance.

The sensitivity to deformation of strain gauges is commonly called GF or strain factor (see SI), and the higher the GF, the better is the strain gauge responsivity. While it is not possible for capacitive isotropic sensors to achieve high GFs as in resistive devices [35, 36], a value higher than the unit can be theoretically obtained for anisotropic dielectrics. Therefore, it is interesting to pursue negative values in a capacitive anisotropic strain gauge, by exploiting auxetic properties. As above mentioned, novel multimodal sensing solutions could be implemented, e.g. a single capacitive sensor could in principle discriminate between a compression imposed on the electrodes (where a capacitance enhancement occurs), and a longitudinal strain (where a capacitance decrease occurs).

We develop a full mathematical model for small tensile strains in z-direction of a capacitive sensor, whose thickness is in x-direction, exploiting an anisotropic foam (see supplementary information, SI) as dielectric. It is shown that an auxetic behavior in at least the thickness direction is necessary for obtaining a negative GF for tensile strain deformations. Briefly, here we introduce the porosity of the foam as

$$\Phi(\varepsilon_z) = (\Phi_0 + \mathrm{M}(\varepsilon_z)\,\Phi_0) \tag{1}$$

where Φ_0 is the porosity before strain and $\Phi(\varepsilon_z)$ is the porosity after a strain ε_z along the direction z and $M(\varepsilon_z)$, the porosity dynamic coefficient, is a parameter dependent with ε_z; the following expression is obtained for a capacitive sensor filled with a dielectric foam:

$$\frac{\Delta C^{\mathrm{FOAM}}(\varepsilon_z)}{C_0^{\mathrm{FOAM}}} = \frac{\Delta C}{C_0} + \mathrm{M}(\varepsilon_z) K \frac{(1+\varepsilon_z)(1-\nu_y\varepsilon_z)}{(1-\nu_x\varepsilon_z)} \tag{2}$$

where $\nu_y = -\varepsilon_y/\varepsilon_z$ and $\nu_x = -\varepsilon_x/\varepsilon_z$, are the Poisson's ratio in the transverse and perpendicular direction ($\nu_y \neq \nu_x$ for anisotropic materials). The first term $\triangle C/C_0$ represents the behavior of a full solid dielectric material, while the second term is the modification due to the porosity and K has the following expression:

$$K = \frac{\Phi_0\left(k_{\mathrm{r}}^{\mathrm{fill}} - k_{\mathrm{r}}^{\mathrm{PM}}\right)}{k_{\mathrm{r}}^{\mathrm{PM}}(1-\Phi_0) + k_{\mathrm{r}}^{\mathrm{fill}}\Phi_0} \tag{3}$$

with $k_{\mathrm{r}}^{\mathrm{fill}}$ is the relative permittivity of the material filling the dielectric pores and $k_{\mathrm{r}}^{\mathrm{PM}}$ is the relative permittivity of the porous material. In case of a negative GF (see SI), the following expression must be satisfied:

$$\nu_x < \frac{1-(1+\varepsilon_z)(1-\nu_y\varepsilon_z)\left[1+\frac{\mathrm{M}(\varepsilon_z)}{\varepsilon_z}K\right]}{\varepsilon_z}. \tag{4}$$

We observe that $\mathrm{M}(\varepsilon_z) < 0$ in case of conventional materials because the porosity decreases under strain while $\mathrm{M}(\varepsilon_z) > 0$ in case of auxetic materials, where the auxetic cells expand with tension, enhancing the porosity $\Phi(\varepsilon_z)$.

3. Materials and methods

3.1. PU foam

PU are a class of polymers whose structure consists of multiple organic compounds derived from carbamic acid (NH_2COOH). We used a reticulated PU foam with a uniform open cell distribution. Reticulation decreases the resistance to compression while increases tensile properties like elongation and resistance to tearing [37].

Several models were developed in the past to describe the mechanical properties of PU cellular materials, depending on, e.g. foam density [38, 39]. One of the most diffused models addressing the micromechanics of 3D open-cell foams is based on tetrakaidecahedral unit cells. In this case, each unit cell has 36 struts treated as uniform slender beams undergoing linearly elastic deformations. The unit cell could also incorporate struts with different cross sectional shapes such as circular, square, equilateral triangle and plateau border [40]. This model explicitly shows that the foam elastic properties depend on the relative foam density, the shape and size of the strut cross section, the Young's modulus and the Poisson's ratio of the strut material.

Conventional sponges with a positive Poisson's ratio and a uniform open cell distribution, such as a reticulated PU foam, are good candidates for the conversion into auxetic ones [25, 26]. In this work, we use this class of materials that have the present lightweight foams, simple to transform into auxetic

structures. The open cell foams (density ≈ 30 kg m^{-3}) (Modulor GmbH®) are characterized by three different values of pores per inch (10, 20 and 60 PPI), representing the density of pores. Anisotropy of the pristine foam plays a strong role on the performance of thermoformed auxetic foams [41], but according Modulor GmbH information, they are a uniform open cell material in the form of 10 mm thick layer sheets. Hence, we mechanically characterized the foams, converted them into auxetic materials, and tested them to verify the role of density in the mechanical properties, in order to choose the best one for our purpose.

3.2. Auxetic anisotropic PU foam fabrication technique

A common PU sponge can be converted into an auxetic one trough a thermal compression process that modifies the regular convex cells in the PU honeycomb structure creating a 3D re-entrant cell topology in which the struts protrude inwardly [42]. The conversion method exploited was based on the compression and heating to a temperature slightly lower than the softening point of the polymeric material at which the cell struts started to collapse. Indeed, at this temperature the struts become viscous and deform inward with a folded shape without starting to liquefy. To permanently set the deformed struts in their new configuration, the compressed foam is then cooled back down to room temperature before removal of the PU foam from the mold [25]. Fabrication parameters for the conversion process were tested in order to investigate in which ways pressure parameters directly affect the auxetization results.

A purposely developed aluminum mold was developed in order to, both, impose an axial compression on the specimens, and modify the regular convex cells in the polymers honeycomb structure creating a 3D re-entrant cell topology (figures 1(a) and (b)). Thick uniform 5 mm walls were made in order to obtain an isotropic heating. Cylindrical shaped pieces of foam (4 cm diameter in figure 1(c) and 5 cm diameter in figure 1(d)) were cut from the starting PU sheets using sharp edge steel cylinders (figure 1(a)). Specimen diameters of $d_{\Phi i} = 4$ cm and $d_{\Phi i} = 5$ cm, same as or slightly larger than the mold diameter, respectively, allowed testing the effects of the different compression force directions. In detail these were: a pure normal compression (perpendicular to the sample circular surface) when the sample diameter is the same as the mold (named as normal compression, (figure 1(c)); and a normal/radial compression through the larger specimen diameter (named as normal/radial compression, figure 1(d)). As schematized in figure 2(a), based on the methods of Sanami and Lakes [28, 43], auxetization experiments were conducted, for each value of the purchased foams (10, 20 and 60 PPI), and for each untreated specimens' diameter ($d_{\Phi i} = 40$ mm and $d_{\Phi i} = 50$ mm—figures 1(c) and (d)). No buckling has been observed during the compression molding. The same temperature ramp but different pressures were used as described below. As a result, different volumetric compression factors V_f/V_i (where V_f and V_i are the initial and final volume, respectively) were obtained, ranging from 1/2 to 1/5, affecting the re-entrancy degree of the struts and the specific Poisson's ratio

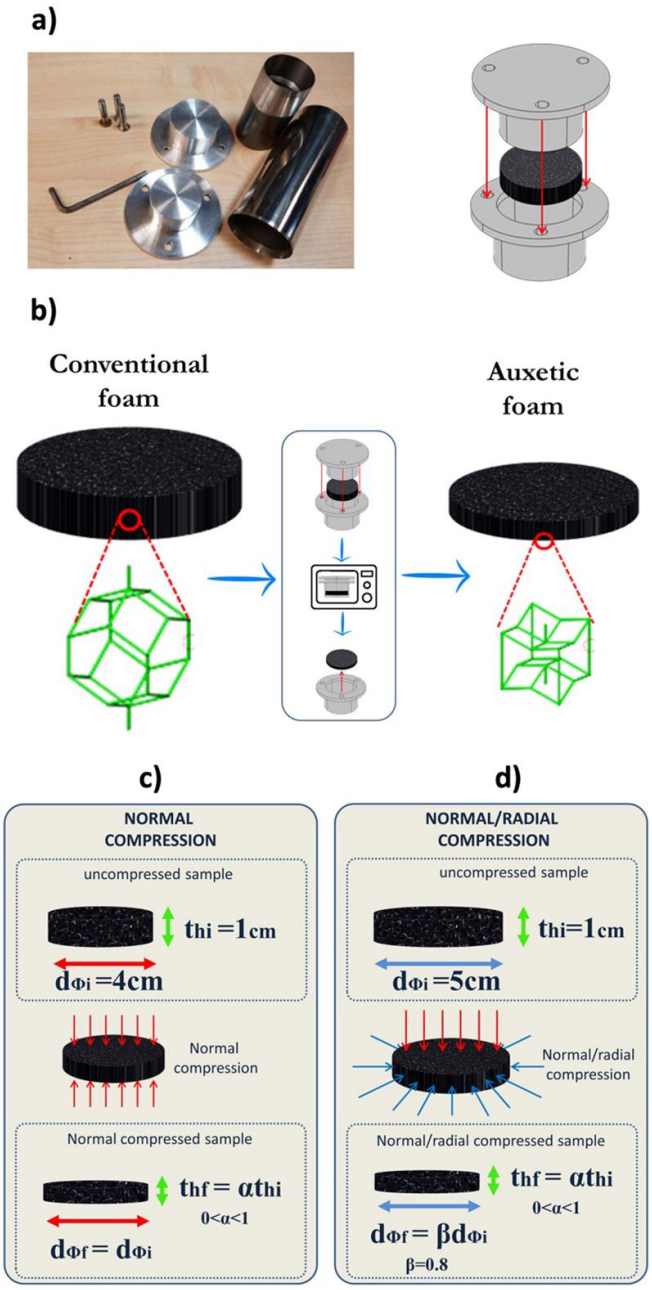

Figure 1. (a) Aluminum mold and sharp edge steel cylinders. (b) Modification in the regular convex cell of the polymer structure after treatment. (c) Pure normal compression: the untreated sample diameter ($d_{\Phi i} = 4$ cm) is the same as the mold diameter, while the compression displacement depends on the normal compression factors α. (d) Normal/radial compression: the untreated sample diameter ($d_{\Phi i} = 5$ cm) is larger than the mold diameter, and a fixed radial compression factor $\beta = 0.8$ is imposed, while the compression displacement depends on the normal compression factors α.

[44]. The inside walls of the mold were lubricated with vegetable or silicone oil and the foam was compressed inside the mold avoiding unwanted creases or torque effect. The piston was then pushed inside it and locked in the desired position. The mold (with the inserted and compressed foams) was then placed into an industrial oven (B180, Nabertherm, Germany),

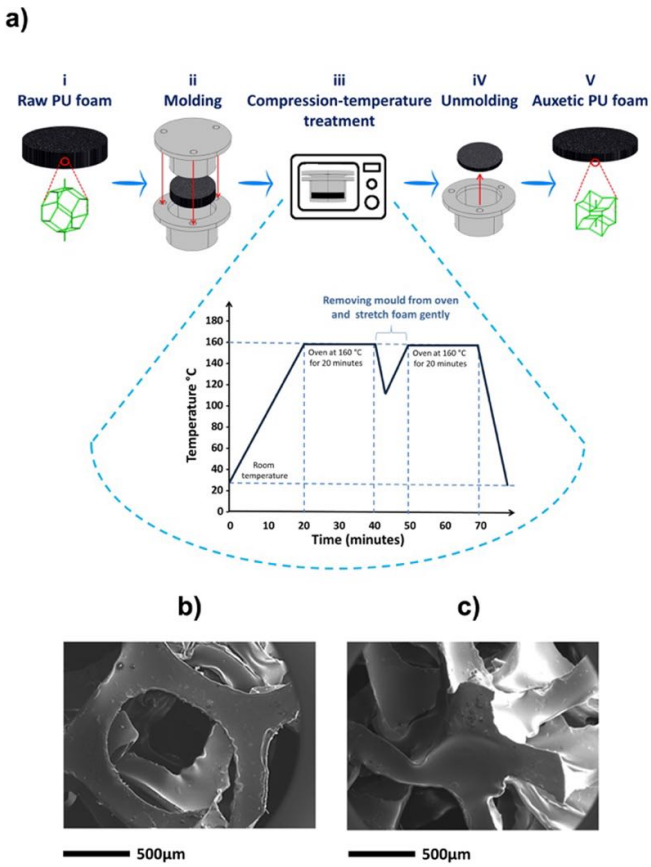

Figure 2. (a) Heating temperature and time profile for manufacturing normal/radial compressed auxetic foams. (b), (c) SEM images of a PU foam specimens: (b) before and (c) after the compression-thermal treatment. The SEM images are related to the 20 PPI treated foam.

heated to a temperature near the softening point of 160 °C (170 °C for the 60 PPI foam) for 20 min, and kept at that temperature for additional 20 min. After removing the mold from the oven, the foam was extracted from it and gently stretched to avoid adhesion of the cell ribs. Then, for a second time the foam was placed into the mold, which was inserted in the oven for 20 min with the same heating ramp as before, in order to permanently set the auxetic deformation. After this, the samples were removed from the mold, cooled at room temperature, and gently tensioned in order to relax the external surface.

Fabricated sponges were visibly auxetic, however many tests were required to determine the Poisson's ratio obtained at different starting configurations. Figures 2(b) and (c) show the scanning electron microscopy (SEM) images of the foam specimens before and after the compression-thermal treatment. The untreated foams have an open-cell structure, and the cell struts are straight while the treated one have the typical deformed configuration. Figures 2(b) and (c) shows cell dimensions are mildly changed and pores number per inch (PPI) are preserved, confirming that the PPI is not changed after treatment.

Table 1. Dimensions of the specimens where d_Φ and *th* represent the diameter and the thickness of the cylinder, respectively, while *L*, *w*, and *th* are the length, the with and the thickness of the cuboid, respectively.

		Compression test (cylinder)		Tension test (cuboid)		
PU	PPI	d_Φ mm	*th* mm	*L* mm	*w* mm	*th* mm
Conventional	10	12.8	10	14	12	10
	20	12.8	10	14	12	10
	60	12.8	10	14	12	10
Auxetic	10	12.8	4,8	14	12	4,8
	20	12.8	3,8	14	12	3,8
	60	12.8	3,4	14	12	3,4

3.3. Mechanical characterizations method

Mechanical and temperature characterizations were performed by a dynamic mechanical analyzer (Q800 DMA, TA Instruments, USA). Flexible PU foam samples with different densities were tested in quasi–static compression and in tension mode. More in details, to investigate the compression and tension stress/strain behavior, measurements were made in a Controlled Force/Strain Rate mode, following a 20 °C isothermal preset ramp. In this mode, the temperature is held constant while strain is ramped at a constant rate without any oscillation frequency in the strain amplitude. In both cases, samples were fixed in the clamp using a dynamometric wrench. Test were made under a DMA controlled preload force of 0,01 N and a constant rate of change of force of 0.2 N min^{-1}. The elastic moduli were measured in the first linear range of the stress–strain curve before the elastic limit was reached. Geometric dimensions of the samples used for the experiments are summarized in table 1. Although the cuboid dimensions, because of experimental limitations, are affected by the Saint Venant effects due to the small scale and the clamping wrench, the compression and traction measurements are a good indication of the order of magnitude of the compression and traction modulus of the pristine and auxetized foam.

3.4. Evaluation of the tensile Poisson's ratio

In order to verify the Poisson's ratio for each starting condition of the auxetization process, and to determine how time, temperature and compression affect the process, the DMA was equipped with two orthogonal cameras (figure 3). The testing set-up consists of two cameras ('AxioCam ERc 5 s' from Carl Zeiss MicroImaging GmbH) in order to measure simultaneously the two transversal deformations with respect to the direction of the force applied to the sample under test in the DMA configured in tension mode. This way we obtain two values of the transverse Poisson's ratio, in the *x*-axis and *y*-axis, respectively. The experimental conditions of the DMA for *x*-axis and *y*-axis Poisson's ratio measurements were the same as in the previous section.

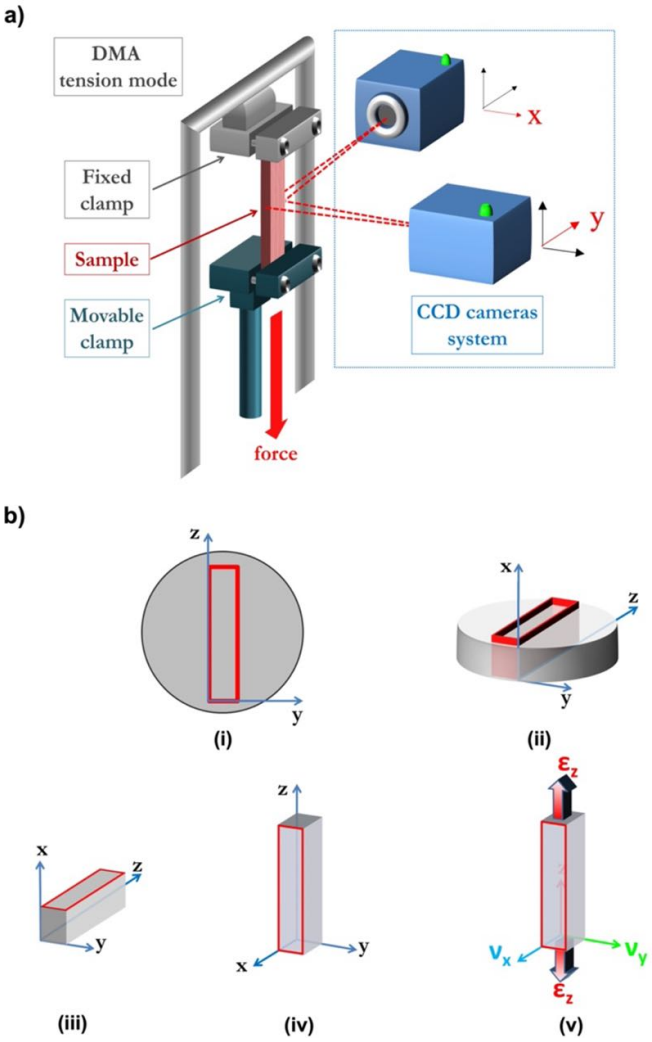

Figure 3. (a) Sketch of the experimental setup for the dynamical mechanic test. Deformations along the x and y axes were simultaneously measured; (b) The reference system for the tensile Poisson's ratio evaluation on the cutted sample from the Polyurethane processed disk. (i) (ii) The circular auxetic sheets of the 20 PPI polyurethane foam. In red there are the cuboid cutting area; (ii) (iv) two different views of the cuboid sample; (v) the cuboid sample will be strained (ε_z) along z axis in order to measure simultaneously the two transversal deformations with respect to the direction of the applied force (z). In this way two values of the transverse Poisson's ratio, in the x-axis (ν_x) and y-axis (ν_y), will be obtained.

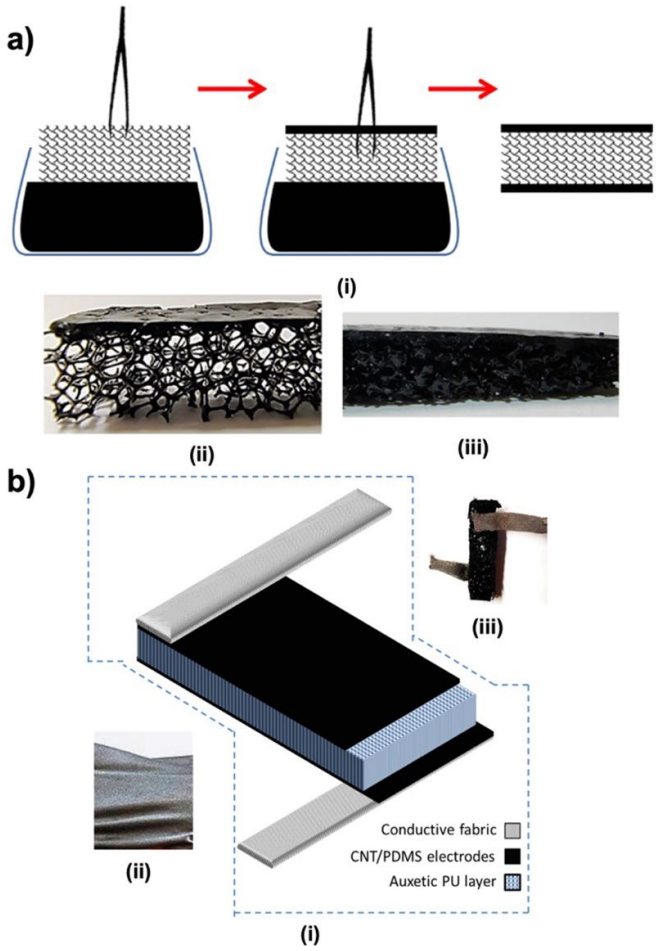

Figure 4. (a) Electrode fabrication: (i) PU was filled with a thin film of uncured CNT/PDMS solution. (ii) Conventional and (iii) auxetic PU with a single conductive layer (on top). (b) Finalized device: (i) Purchased conductive fabric; (ii) 3D representation of device; (iii) fabricated sensor.

3.5. Auxetic PU foam-based capacitive strain gauge sensor fabrication

In a previous work [30] from our group, the fabrication process of a flexible CNTs-based auxetic electrode, suitable for soft sensors and devices, was addressed; it will be briefly outline here. In order to characterize the PU foam as a dielectric for capacitive sensing, a thin top/bottom surface layer of the porous PU was filled with a pristine CNT/PDMS/methyl group-terminated PDMS (MEP) conductive paste, later cured in oven for 30 min at 80 °C (figure 4(a)(i)). These two conducting layers work as top and bottom electrodes. The used materials were the following: functionalized Graphitized Multi Walled CNT (Purity >99.99%, outer diameter 18–28 nm) (Nanocyl SA, Belgium); PDMS and MEP (Dow Corning, Midland, MI, USA). All chemicals, including isopropyl alcohol (IPA) and other organic solvents, were obtained at high-performance liquid chromatography grades with >99.9% purities (Sigma-Aldrich, St. Louis, MO, USA).

Pristine CNT were first dispersed in IPA with a 100:1 weight ratio; strongly aggregated CNT bundles were temporarily separated and stabilized by sonication and the gaps between them were then coated and filled with the IPA solvent at the frequency of 35 kHz and the power of 80 W for 30 min. 20% wt of MEP with low viscosity (100 cSt) was added to the CNT-dispersed IPA solution and blended for 15 min by sonication. MEP is a non-volatile polymeric organosilicon material which penetrates the IPA phase in individual CNT/IPA complexes and adheres to the 80% wt of the base of the Sylgard 184 silicone elastomer (PDMS-A, viscosity of 3500 cSt) was then blended with the CNT/IPA/MEP solution by sonication. Both PDMS-A and CNT/MEP become stable and aggregate in single CNT/IPA/MEP/PDMS-A units in the IPA solution because PDMS-A could make direct contact with the MEP

phase and surround the CNT. After the complete removal of the IPA components, slowly vaporizing at 50 °C hot plate, only the CNT/MEP/PDMS-A units remain. The curing agent from the Sylgard 184 silicone elastomer kit, named PDMS-B, with a 15:1 weight ratio is then added and mixed. As highlighted in figures 4(a)(ii) and (iii), the conductive silicone was inserted by dipping into approximately 1 mm of the foam surface, covering all fibers and filling hollow space of the cell structures. In this way, the stretchable silicone conductor was stably bonded with the foam fibers making a large electrode area and providing a compliant, strong mechanical connections both in conventional and auxetic PU foam. Figure 4(b)(i) shows a schematic with the foam equipped with the compliant electrode. A small drop of uncured CNT/PDMS was used as conductive adhesive to glue the foam electrodes to a stretchable conductive fabric coated with a medical grade silver layer (Holland Shielding Systems B.V.) (figure 4(b)(ii)), ensuring an electric connection with an inductance (L), capacitance (C), and resistance (R) meter (LCR) meter probes. In figure 4(b)(iii) the final fabricated sensor is shown. Because of the mechanical characterization in the small strain regime, no cracks in the flexible carbon nanotubes-based auxetic electrode have been observed.

4. Results and discussion

4.1. Conventional PU foam compression and tension characterization

For the conventional open cells foam, the stress–strain relationships of three tested samples (three for each foam type: 10 PPI, 20 PPI and 60 PPI) are shown in figures 5(a) and (b). Under compression and tension, a typical stress–strain response for elastomeric foams [45] is observed. Compressive stress–strain behavior starts with the linear region of elasticity, where Hooke's law applies and it is possible to evaluate the modulus of elasticity, and the strain energy is stored in reversible bending of the struts. A plateau follows, where struts begin to impinge upon each other, and, finally, a densification region where the foam at this stage becomes a virtual solid material: the cells are completely flattened causing a sudden increase in internal compression stiffness of the cellular network. Tensile stress–strain responses show a behavior that depends on different materials and significantly differ for the various densities of PU foams. The obtained results for the quasi static modulus are in agreement with previous literature [46].

4.2. Auxetic PU foam compression and tension characterization

Figures 5(c) and (d) presents the stress–strain behavior under compression and tension of the auxetic samples. The results, typical of auxetic foams [47, 48], show an increase in stiffness during compressive loading: it is possible to observe two distinct phases, namely, an initial, soft phase and a final, stiff phase. The two phases are connected by a gradual stiffening due to a densification phase described by a super-linear increase. Tensile stress–strain responses show a behavior that resembles that of conventional materials but show a significant increase with respect to that of the conventional PU foam studied in the previous sections. Table 2 presents a summary of the results of the test for each type of foam, conventional or auxetic, at different density, 10, 20 and 60 PPI. From the results of our experimental analysis, we chose a foam density of 20 PPI for the Poisson's test characterization.

4.3. Evaluation of the tensile Poisson's ratio of fabricated auxetic PU foam

Circular auxetic sheets of the 20 PPI PU foam were cut in a cuboid shape (figure 3(b)) for both normal compressed and normal/radial compressed PU sponges.

For the normal auxetized PU sample (figure 1(c)), the variation of Poisson's ratio with the increase in vertical strain ε_z can be observed in figures 6(a) and (b). The auxetic foam exhibits a negative Poisson's ratio in the x direction until approximately 15% of the axial strain and then saturates to a negligible value in the range between 15% and 25%, finally showing a conventional positive value (figure 6(a)). This phenomenon depicts the gradual recovery of conventional behavior at higher axial strain levels [49]. In contrast, the Poisson's ratio of the same auxetic PU foam into the y direction was positive (figure 6(b)) throughout the loading, showing a conventional linear behavior. In the case of normal/radial (figure 1(d)) auxetization processing both x and y strain variation exhibited a negative Poisson's ratio with the increase in vertical strain ε_z and can be observed in figures 6(c) and (d). For both strain variations, the auxetic foam exhibited a negative Poisson's ratio until approximately 25% of the axial strain and then deviates this behavior to a conventional positive value [49].

In conclusion, figures 6(a)–(d) shows that the auxetic effect for the converted foams occurs over a specific tensile strain before undergoing a transition to positive Poisson's ratio foam. The results for both types of samples confirm that the PU conventional sponge samples after the thermal-compression process exhibit an auxetic behavior. Furthermore, while normal compressed samples shown a conventional behavior into the y-direction and an auxetic behavior into the transversal one ($\nu_x = -0,80 - \nu_y = 0,22$), normal/radial compressed samples are auxetic in both x- and y- directions ($\nu_x = -1,03 - \nu_y = -0,2$). To design a capacitive-based strain sensor (figure 6(e), where electrode area is highlighted), capacitance variations need to be dependent only from the dielectric thickness changes, while the area of the electrodes should have negligible change under strain. In fact, due to a positive strain ε_z in z direction, both normal compressed and normal/radial compressed auxetized foams increase the thickness in x-direction but differences along y-directions are showed, instead: while in the normal compressed auxetized case the electrode shrinks in the y-direction (figure 6(f)), in the normal/radial compressed auxetized case the electrodes area broadens in the y-direction (figure 6(g)). Only normal compressed auxetization process is investigated for our capacitive strain gauge fabrication. In this case, the changes in the y-z plane electrode total area can be considered negligible (figure 6(f)) in first approximation; to investigate a $GF^{\mathrm{FOAM}} < 0$ strain gauge, therefore, only the

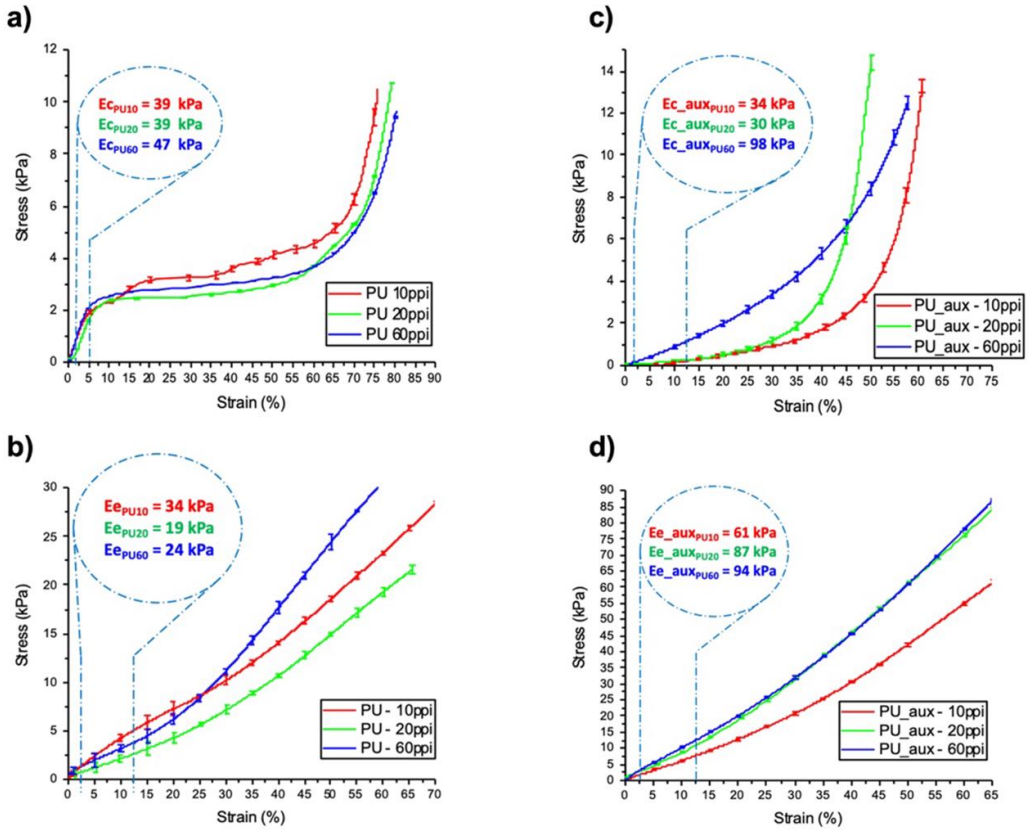

Figure 5. PU conventional foam DMA: (a) compression and (b) tension stress–strain responses performed at three densities (10, 20, 60 PPI) of the sponge; PU auxetic foam DMA: (c) compression and (d) tension stress–strain responses performed at three densities (10, 20, 60 PPI) of the sponge.

Table 2. Summary of the results of the test. In bold are highlighted the 20PPI foam selected for device fabrication.

		Conventional PU	Auxetic PU
PU	PPI	(kPa)	(kPa)
Compression	10	39	34
	20	**39**	**30**
	60	47	98
Tension	10	34	61
	20	**19**	**87**
	60	24	94

normal compressed auxetized 20 PPI PU foam will be tested as dielectric in the capacitive sensor.

4.4. Auxetic PU foam-based capacitive strain gauge sensor electrical behavior

Figure 7 shows the electrical response of the capacitive strain gauge sensor under tensile strain for conventional and normal compressed auxetized capacitive sensor. To calculate the dynamic coefficient $M(\varepsilon_z)$, PU (PM stays for porous material and ST for standard material) and 'air filler' parameters from datasheet and literature [50] were exploited,

$$k_{\mathrm{r}}^{\mathrm{fill}} = 1 \quad k_{\mathrm{r}}^{\mathrm{PM}} = 6.4$$

$$\rho_{\mathrm{PM}}^{*} = 30\ {}^{Kg}/_{m^3} \quad \rho_{\mathrm{ST}} = 1220\ {}^{Kg}/_{m^3}$$

and the parameters Φ_0 and K for the conventional case and the normal compressed auxetic foams were evaluated. The results are reported in table 3.

In figure 7(a)(i) the foam-based flexible capacitance conventional sensor behavior under longitudinal strain (z-direction) is shown and present a linear increasing of the capacitance with the strain due to the thickness reduction (x-direction) of the dielectric layer. A GF of 1.1 was measured. Applying equation (2) for calculating the numerical expression of the porosity dynamic coefficient $M(\varepsilon_z)$, we obtain a decreasing linear fit and negative values, as expected, with a slope equals to $-190\,562$ (figure 7(a)(ii)).

In contrast, figure 7(a)(iii) shows relative capacitance changes with z-direction tensile strain in the case of the auxetic PU foam dielectric. Due to the normal auxetic behavior, for strain values up to 10% the capacitance decreases because of electrodes distance increases (figure 7(a)(iii) inset). In this range, the measured Gf is negative and equals to -2.8, and as expected its magnitude is distinctly higher than the unity. For strains larger than 10%, the capacitance starts to increase according to the conventional behavior: this happens because the corrugated ribs of the auxetic cells reach the expansion limit. Therefore, for strain values in the range of 10%–20% (figure 7(a)(iii)), the conventional behavior recovers, and a positive Poisson's ratio value is obtained. For

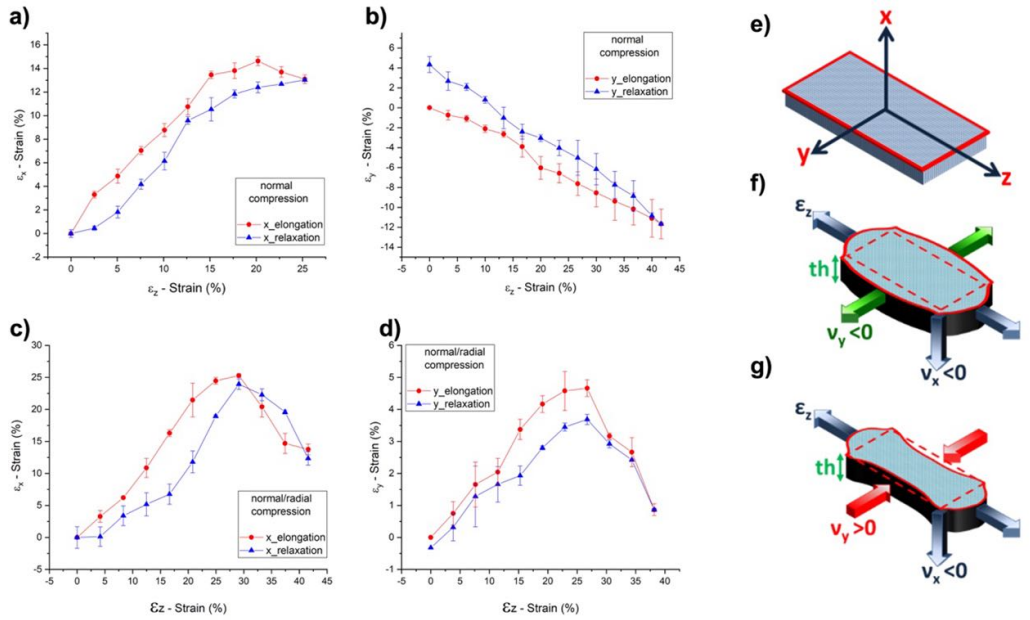

Figure 6. Tests on cuboid auxetic sheets of the 20 PPI polyurethane foam: (a) Strain along x vs Strain along z for the 20 PPI normal compressed auxetic PU foam. Poisson's ratio along the x direction: Elongation: $\nu_x = -0{,}80$ (red line); relaxation: $\nu_x = -0{,}86$ (blue line); (b) Strain along y vs Strain along z for the 20 PPI normal compressed auxetic PU foam. Poisson's ratio along the y direction: Elongation: $\nu_y = 0{,}22$ (red line); relaxation: $\nu_y = 0{,}41$ (blue line); (c) Strain along x vs Strain along z for the 20 PPI normal compressed auxetic PU foam. Poisson's ratio along the x direction: Elongation: $\nu_x = -1{,}03$ (red line); relaxation: $\nu_x = -0{,}57$ (blue line); (d) Strain along y vs Strain along z for the 20 PPI normal compressed auxetic PU foam. Poisson's ratio along the y direction: Elongation: $\nu_y = -0{,}2$ (red line); relaxation: $\nu_y = -0{,}16$ (blue line). Cuboid auxetic samples area changes with the strain: (e) undeformed specimen and space coordinate system; (f) normal compressed case: the changes in the electrodes area can be negligible because the sample is lengthened in z-direction and shrinked in the y-direction; (g) normal/radial compressed case: the electrodes area increases because the sample is lengthened in z-direction and broadened in the y-direction.

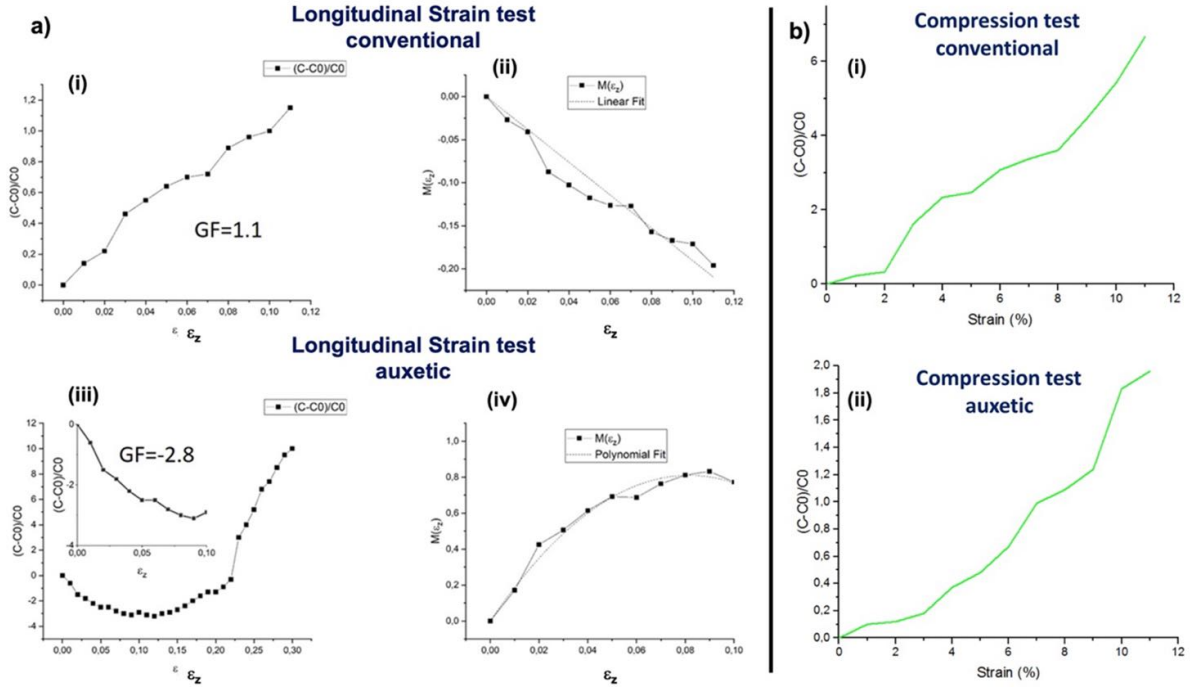

Figure 7. (a) Foam-based flexible capacitance behavior test under tensile strain: (i) test for the conventional sensor under longitudinal strain; (ii) related porosity dynamic coefficient M(ε_z) for conventional sensor with decreasing linear fit; (iii) test for the auxetic sensor under longitudinal strain; (iv) related porosity dynamic coefficient M(ε_z) for auxetic sensor with decreasing second order polynomial fit.
(b) Foam-based flexible capacitance behavior test under compression stress for (i) the conventional sensor and for (ii) the auxetic sensor.

Table 3. Evaluated Φ_0 and K parameters for the conventional case and for the two different auxetic foam.

	$\Phi_0 = 1 - \frac{\rho^*_{PM}}{\rho_{ST}}$	$K = \frac{\Phi_0\left(k_r^{fill} - k_r^{PM}\right)}{k_r^{PM}(1-\Phi_0)+k_r^{fill}\Phi_0}$
Conventional PU	$\Phi_0 = 0,98$	$K = -4,78$
Normal compression	$\Phi_0 = 0,92$	$K = -3,47$

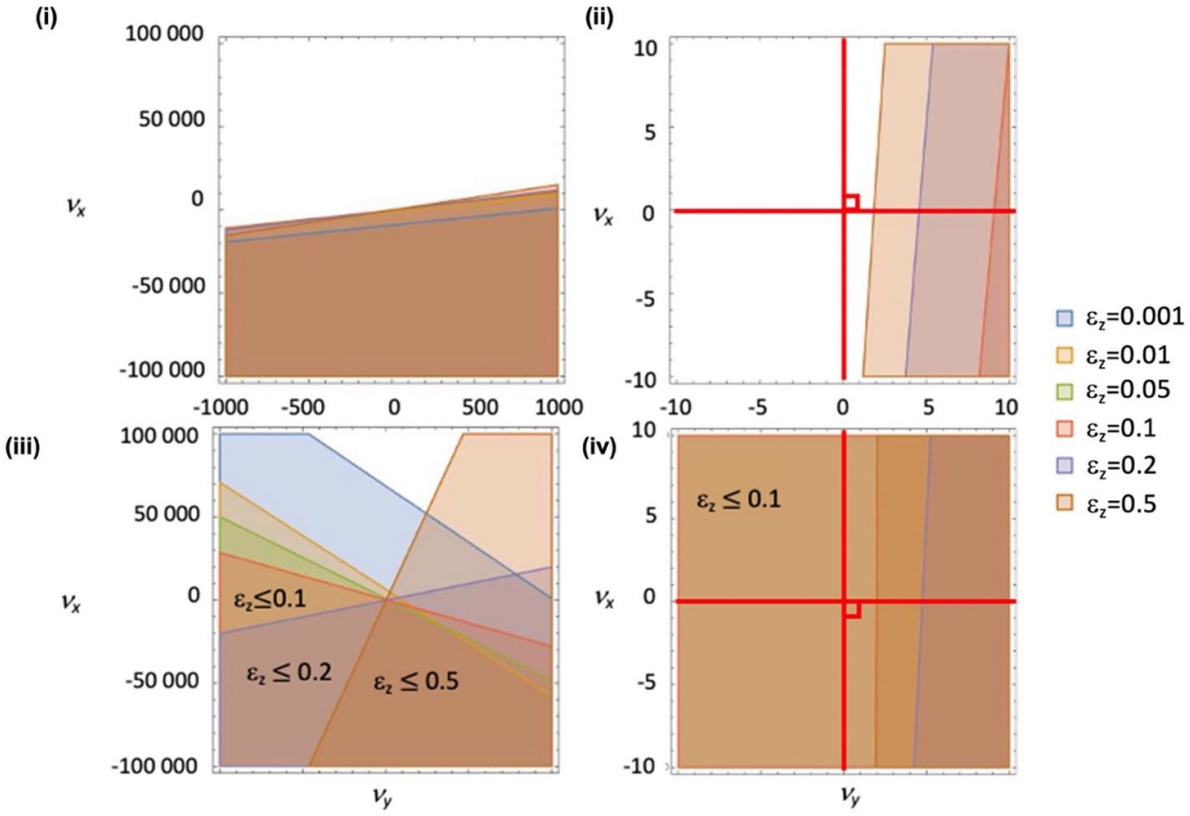

Figure 8. Left column: Poisson's ratio values in x- and y-directions that solve inequality (4) for the (i) conventional foam, (iii) the auxetic-normal compressed foam. The parameter ε_z is the applied strain along z. Right column: graphical zoom of left graphics for Poisson's ratios values $|\nu_y| < 10$ and $|\nu_x| < 10$: (ii) The red square highlights the conventional region $0 < \nu_x < 0.5$ and $0 < \nu_y < 0.5$. The conventional PU foam falls in this region ($\nu_x = \nu_y = 0.3$), where inequality (4) is not satisfied; (iv) The red square highlights the region $-1 < \nu_x < 0$ and $0 < \nu_y < 0.5$ where the Poisson's ratio of the normal compressed auxetic PU foam falls ($\nu_x = -0.80 - \nu_y = 0.22$) showing the inequality (4) is satisfied up to $\varepsilon_z < 0.1$.

the normal compressed auxetic foam, the expression of the porosity dynamic coefficient $M(\varepsilon_z)$ shows positive values and is no longer linear but follows a second order polynomial fit ($M(\varepsilon_z) = 19.87735\ \varepsilon_z - 121.94486\ \varepsilon_z^2$) in the region until $\varepsilon_z < 0.1$, where the negative GF is obtained (figure 7(a)(iv)). Figure 7(b) shows the same behavior for compression tests on both conventional (figure 7(b)(i)) and auxetic capacitors (figure 7(b)(ii)). As expected, the decrease in the dielectric layer thickness generates an enhancement of capacitance with the compression. This variation is higher for conventional foam than normal compressed auxetic foam. In fact, the auxetic treatment makes the ribs already corrugated along z- direction limiting the relative variation of the capacitance. This kind of behavior demonstrates the different strain measurement modalities (compression/tension) that are possible. A foam-based flexible auxetic capacitance sensor based on our material could then discriminate between compression (where a positive output variation occurs) and tension (with a negative output variation) up to 10% tensile strain.

4.5. Experimental validation of the developed mathematical model

In order to confirm the theoretical model for a negative Poisson's ratio auxetic material, inserting the measured Poisson's ratios and the fitted expression of $M(\varepsilon_z)$, equation (4) has to be verified for the capacitive strain gauge filled with the 20 PPI normally compressed auxetic PU dielectric and not verified for the standard PU material. Through table 3 values and taking the strain along z (ε_z) as a parameter, figure 8 shows for each considered strain, in colored area, the Poisson's ratio values in x- and y-directions that solve inequality (4). Figures 8(i) and (iii) show inequalities related to conventional and normal compressed auxetic, respectively. It is possible to graphically

evaluate which is the set of Poisson's ratios along x- and y-directions able to solve (4) in a large range of strain along z-direction until $\varepsilon_z = 0.5$. Figures 8(ii) and (iv) show a zoom of the region around $(\nu_y, \nu_x) = (0,0)$ where two orthogonal red lines separate the quadrants with different signs for the Poisson's ratio along x- and y-directions. In figure 8(ii) the conventional foam region ($\nu_x > 0$ and $\nu_y > 0$) is highlighted and a squared shape shows the conventional range ($0 < \nu_x < 0.5$ and $0 < \nu_y < 0.5$). It is possible to observe that the standard Poisson's ratios of the conventional PU foam (expected in the range between 0 and 0.5) make $GF^{\mathrm{FOAM}} < 0$ impossible for each strain. As shown in figure 8(iv), in case of the normal auxetized foam ($-1 < \nu_x < 0$ and $0 < \nu_y < 0.5$, see the squared shape), the measured Poisson's ratios for the 20 PPI PU foam fall in this area ($\nu_x = -0.80$ – $\nu_y = 0.22$). In this case, $GF^{\mathrm{FOAM}} < 0$ is possible for z-direction strain ranging up to $\varepsilon_z = 0.1$. For higher values, the condition (4) is no longer holding. This is confirmed by the experimental measurements showed earlier in figure 7(a).

5. Conclusions

In this work, auxetic PU foams exhibiting a negative Poisson's ratio are prepared by thermo-mechanical auxetic conversion from an open cell PU foam. The auxetic behavior is modeled and conditions for a negative GF in an auxetic capacitive strain gauge are studied. It is shown that a range of negative Poisson Ratio's values in different geometric directions can be exploited for multimodal tactile applications based on negative GF values. To the best of our knowledge, this is the first time that a theoretical description of an auxetic dielectric capacitive strain gauge is proposed.

Based on such encouraging results we combine our auxetic anisotropic PU foam with CNT/PDMS conductive composite electrodes and develop a soft capacitive strain gauge. Electromechanical characterizations demonstrate a negative GF equal to -2.8 for tensile strain and an increase of capacitance for compressive strain. Finally, we report the experimental validation of our proposed model. In a forthcoming work, this model will be carefully tested in a final capacitive strain gauge, in order to measure the GF under actual conditions. Moreover, this will allow to test this potential auxetic foam-based multimodal capacitive strain gauge on a larger number of fabricated devices and through ageing tests.

In the near future we plan to exploit our results to design auxetic soft strain sensors in which, depending on the externally applied stimuli, e.g. force direction, a normally applied force can be discriminated from a tensile force by means of the different electrical behavior. We believe that our methodology can represent the basis for an improved design freedom for multimodal mechanical soft sensors and that innovative effective designs will be possible for sensors to discriminate among different mechanical stimuli. In this vision, these results set an opportunity towards smart wearables and the development of perceptive soft robots in which the sensing structures, although merged with the soft body are required to provide information about the deformations induced by external stimuli (tactile) as well as the internal ones, i.e. those provoked by the actuation of the robot itself.

Data availability statement

The data that support the findings of this study are available from the corresponding author upon reasonable request.

ORCID iDs

F Rizzi https://orcid.org/0000-0002-5142-5231
S Puce https://orcid.org/0000-0002-1745-9163
F La Malfa https://orcid.org/0000-0001-7345-0406
M Totaro https://orcid.org/0000-0002-0630-7383
M De Vittorio https://orcid.org/0000-0003-1601-6392
L Beccai https://orcid.org/0000-0002-8754-5155

References

[1] Lakes R S 2017 Negative-Poisson's-ratio materials: auxetic solids *Annu. Rev. Mater. Res.* **47** 63–81
[2] Kolken H M A and Zadpoor A A 2017 Auxetic mechanical metamaterials *RSC Adv.* **7** 5111–29
[3] Mousanezhad D, Babaee S, Ebrahimi H, Ghosh R, Hamouda A S, Bertoldi K and Vaziri A 2015 Hierarchical honeycomb auxetic metamaterials *Sci. Rep.* **5** 18306
[4] Scarpa F, Giacomin J, Zhang Y and Pastorino P 2005 Mechanical performance of auxetic polyurethane foam for antivibration glove applications *Cell. Polym.* **24** 253–68
[5] Alderson A and Alderson K L 2007 Auxetic materials *Proc. Inst. Mech. Eng.* G **221** 565–75
[6] Yang W, Li Z-M, Shi W, Xie B-H and Yang M-B 2004 Review on auxetic materials *J. Mater. Sci.* **39** 3269–79
[7] Choi J B and Lakes R S 1991 Design of a fastener based on negative Poisson's ratio foam *Cell. Polym.* **10** 205–12
[8] Ren X, Shen J, Tran P, Ngo T D and Xie Y M 2018 Auxetic nail: design and experimental study *Compos. Struct.* **184** 288–98
[9] Morvan O, Manuel C and Fabrizio S 2016 A piezo-shunted kirigami auxetic lattice for adaptive elastic wave filtering *Smart Mater. Struct.* **25** 115016
[10] Mir M, Ali M N, Sami J and Ansari U 2014 Review of mechanics and applications of auxetic structures *Adv. Mater. Sci. Eng.* **2014** 17
[11] Alderson J R A, Evans K E and Grima J N 2001 Auxetic polymeric filters display enhanced de-fouling and pressure compensation properties *Membr. Technol.* **2001** 6–8
[12] Alderson A 1999 A triumph of lateral thought *Chem. Ind.* **17** 384–91
[13] Hotzen I, Ternyak O, Shmulevich S and Elata D 2015 Mass-fabrication compatible mechanism for converting in-plane to out-of-plane motion *2015 28th IEEE Int. Conf. on Micro Electro Mechanical Systems (MEMS)* pp 897–900
[14] Rafsanjani A and Bertoldi K 2017 Buckling-induced kirigami *Phys. Rev. Lett.* **118** 084301
[15] Zega V, Bruggi M, Levi M and Corigliano A 2015 Auxetic materials for MEMS: modeling, optimization and additive manufacturing *AIMETA 2015* (*Genova*) pp 489–97
[16] Wang H, Totaro M and Beccai L 2018 Toward perceptive soft robots: progress and challenges *Adv. Sci.* **5** 1800541
[17] Kang M, Kim J, Jang B, Chae Y, Kim J-H and Ahn J-H 2017 Graphene-based three-dimensional capacitive touch sensor for wearable electronics *ACS Nano* **11** 7950–7

[18] Yu H, Lian Y, Sun T, Yang X, Wang Y, Xie G, Du X, Gou J, Li W and Tai H 2019 Two-sided topological architecture on a monolithic flexible substrate for ultrasensitive strain sensors *ACS Appl. Mater. Interfaces* **11** 43543–52

[19] Taherkhani B, Azizkhani M B, Kadkhodapour J, Anaraki A P and Rastgordani S 2020 Highly sensitive, piezoresistive, silicone/carbon fiber-based auxetic sensor for low strain values *Sens. Actuators* A **305** 111939

[20] Clemens F, Melnykowycz M, Bär F, Goldenstein D and Georgopoulou A 2021 2D printing of piezoresistive auxetic silicone sensor structures *IEEE Robot. Autom. Lett.* **6** 2541–6

[21] Wang Z, Luan C, Liao G, Liu J, Yao X and Fu J 2021 High-performance auxetic bilayer conductive mesh-based multi-material integrated stretchable strain sensors *ACS Appl. Mater. Interfaces* **13** 23038–48

[22] Lee Y-J, Lim S-M, Yi S-M, Lee J-H, Kang S-G, Choi G-M, Han H N, Sun J-Y, Choi I-S and Joo Y-C 2019 Auxetic elastomers: mechanically programmable meta-elastomers with an unusual Poisson's ratio overcome the gauge limit of a capacitive type strain sensor *Extreme Mech. Lett.* **31** 100516

[23] Shintake J, Nagai T and Ogishima K 2019 Sensitivity improvement of highly stretchable capacitive strain sensors by hierarchical auxetic structures *Front. Robot.* AI **6** 127

[24] Liu H, Laflamme S, Li J, Bennett C, Collins W, Downey A, Ziehl P and Jo H 2021 Soft elastomeric capacitor for angular rotation sensing in steel components *Sensors* **21** 7017

[25] Lim T-C 2015 *Auxetic Materials and Structures* 1st edn (Singapore: Springer)

[26] Lisiecki J, Błażejewicz T and Kłysz S 2010 Flexible auxetic foams—fabrication, properties and possible application areas *Research Works of Air Force Institute of Technology* **27** 57

[27] Li Y and Zeng C 2016 On the successful fabrication of auxetic polyurethane foams: materials requirement, processing strategy and conversion mechanism *Polymer* **87** 98–107

[28] Friis E A, Lakes R S and Park J B 1988 Negative Poisson's ratio polymeric and metallic foams *J. Mater. Sci.* **23** 4406–14

[29] Zhang S L, Lai Y-C, He X, Liu R, Zi Y and Wang Z L 2017 Auxetic foam-based contact-mode triboelectric nanogenerator with highly sensitive self-powered strain sensing capabilities to monitor human body movement *Adv. Funct. Mater.* **27** 1606695

[30] La Malfa F, Puce S, Rizzi F and De Vittorio M 2020 A flexible carbon nanotubes-based auxetic sponge electrode for strain sensors *Nanomaterials* **10** 2365

[31] Liu H *et al* 2020 Numerical investigation of auxetic textured soft strain gauge for monitoring animal skin *Sensors* **20** 4185

[32] Liu H, Laflamme S, Li J, Bennett C, Collins W, Downey A, Ziehl P and Jo H 2021 Investigation of surface textured sensing skin for fatigue crack localization and quantification *Smart Mater. Struct.* **30** 105030

[33] Casavola C, Del Core L, Moramarco V, Pappalettera G and Patronelli M 2021 Experimental and numerical analysis of the Poisson's ratio on soft polyurethane foams under tensile and cyclic compression load *Mech. Adv. Mater. Struct.* **29** 7172–88

[34] Stockmann M, Naumann J and Ihlemann J 2017 25 years basic research in the field of strain gage technology on Chemnitz University of technology—institute of mechanics ed EUT Edizioni Università di Trieste

[35] Zeiser R, Fellner T and Wilde J 2014 Capacitive strain gauges on flexible polymer substrates for wireless, intelligent systems *J. Sens. Sens. Syst.* **3** 77–86

[36] Shintake J, Piskarev E, Jeong S H and Floreano D 2018 Ultrastretchable strain sensors using carbon black-filled elastomer composites and comparison of capacitive versus resistive sensors *Adv. Mater. Technol.* **3** 1700284

[37] 1967 *Cellular Plastics: Proceedings of a Conference* (ed) Kurt C Frisch (Washington, DC: The National Academies Press) (https://doi.org/10.17226/21280)

[38] Alzoubi M, Al-Waked R and Tanbour E 2011 Compression and hysteresis curves of nonlinear polyurethane foams under different densities, strain rates and different environmental conditions *J. Mech. Eng.* **9** 101–9

[39] Saha M, Mahfuz H, Chakravarty U, Uddin M and Jeelani S 2005 Effect of density, microstructure, and strain rate on compression behavior of polymeric foams *Mater. Sci. Eng.* A **406** 328–36

[40] Li K, Gao X-L and Roy A K 2005 Micromechanical modeling of three-dimensional open-cell foams using the matrix method for spatial frames *Composites* B **36** 249–62

[41] Zhang Q, Yu X, Scarpa F, Barton D, Rankin K, Lang Z-Q and Zhang D 2022 Anisotropy in conventional and uniaxially thermoformed auxetic polymer foams *Composites* B **237** 109849

[42] Chan N and Evans K E 1997 Fabrication methods for auxetic foams *J. Mater. Sci.* **32** 5945–53

[43] Sanami M, Ravirala N, Alderson K and Alderson A 2014 Auxetic materials for sports applications *Proc. Eng.* **72** 453–8

[44] Liu Y and Hu H 2010 A review on auxetic structures and polymeric materials *Sci. Res. Essays* **5** 1052–63

[45] Razmara M, Saidpour S H and Arunchalam S 2008 DMA Investigation on polyurethane (PUR) *Int. Conf. on Fascinating Advancement in Mechanical Engineering (FAME 2008)* (Sivakasi: Mepco Schlenk Engineering College)

[46] Alzoubi M, Al-Hallaj S and Abu-Ayyad M M 2014 Modeling of compression curves of flexible polyurethane foam with variable density, chemical formulations and strain rates *J. Solid Mech.* **6** 82–97

[47] Scarpa F 2008 Auxetic materials for bioprostheses [In the Spotlight] *IEEE Signal Process. Mag.* **25** 128–126

[48] Scarpa F and Malischewsky P G 2008 Some new considerations concerning the Rayleigh-wave velocity in auxetic materials *Phys. Status Solidi* b **245** 578–83

[49] Zahra T and Dhanasekar M 2017 Characterisation of cementitious polymer mortar—auxetic foam composites *Constr. Build. Mater.* **147** 143–59

[50] Petrossian G, Hohimer C and Ameli A 2019 Highly-loaded thermoplastic polyurethane/lead zirconate titanate composite foams with low permittivity fabricated using expandable microspheres *Polymers* **11** 280